ADVANCED OPTICAL MATERIALS
www.advopticalmat.de

Dynamic Augmented Reality Display by Layer-Folded Metasurface via Electrical-Driven Liquid Crystal

*Jiao Tang, Shuai Wan, Yangyang Shi, Chengwei Wan, Zejing Wang, and Zhongyang Li**

Heading toward the next-generation versatile meta-devices and meta-systems with increasing complexity, it inevitably demands the cascading and coupling between multi-layer metasurfaces to create new design space for meta-optics. However, the accurate requirement for multilayer alignment at the nanoscale is significantly challenging due to the actual fabrication limitation, thus hindering the state-of-the-art meta-optics device integration and its practical application. Herein, a dynamic meta-system for augmented reality (AR) holographic display functionality based on a layer-folded metasurface integrated with an electrical-driven liquid crystal (LC) platform is originally proposed and realized. By ingeniously folding the optical path between meta-device vertical space, a beam-steering metasurface in parallel with the other two holographic metasurfaces placed on a single surface is successfully cascaded. Such a layer-folded scheme enjoys single-time lithography processing for multi-patterning with nanoscale alignment accuracy and avoids any vertical alignment issue. Furthermore, by combining with an electrical-driven LC tuning scheme, the integrated meta-system could actively switch independent-encoded holographic images in real-time floating in the actual-world scene. Overall, it is envisioned that such a compact dynamic meta-system suggests a feasible route for dynamic tunable wearable AR displays, intelligent dynamic displays, multi-functional devices, etc.

1. Introduction

The invention of metasurfaces creates new degrees of freedom to control light at the subwavelength resolution and emerges as a promising platform for novel optical meta-devices and meta-systems. Various fascinating functionalities have been achieved by single-layer metasurface design, including perfect absorber,[1,2] nanoprinting display,[3–5] beam steering,[6,7] metalens,[8,9] meta-holography,[10–18] and many others.[19,20] However, heading toward the development and achievement of more powerful meta-devices and even more complicated meta-systems, it inevitably demands the cascading and coupling between multi-layer metasurfaces as a feasible design strategy.[21–25] Multi-layer metasurface possesses more degrees of freedom for light manipulation, which provides a more powerful method to overcome the drawbacks of the single-layer metasurface. For instance, by utilizing dual-layered metasurface cooperation, an optical retroreflector[26] has been demonstrated beyond the single-layered metasurface functionality. Moreover, based on multi-layer coupling and tuning between metasurfaces, it expands the multiplexing channels and creates new degrees of freedom for holographic display performance. This includes the demonstration of dual-band vectorial metahologram,[27] multicolor holography,[28] cascaded hologram,[29] and so on. Despite its significant potential and capability, one of the most critical challenges for multilayered metasurface realization is the accurate alignment between layers in the actual fabrication.[30] Typically, it requires microscale or even nanoscale precise alignment due to the cooperative coupling demand for shaping wavefront at the subwavelength scale, which hinders the state-of-the-art meta-optics capability and its practical application. To conquer the alignment difficulty, the ingeniously folding the vertical optical path by the total internal reflection (TIR) to coupling and integrating multi-metasurface parallel onto a single chip, that is, layer-folded metasurface[31,32] would suggest a new route for single-time lithography convenience in nanofabrication and conquer the vertical alignment challenge in multi-patterning. On the other hand, in the evolutionary trend toward the intelligent optical device, dynamic tunability is also essential to meta-device functionality. Various dynamic mechanisms, including electrical[11,33–37]/thermal[38–40]/mechanical[41]/optical tuning[42] schemes, have been investigated to exhibit switchable optical performance. Among the main active modulation methods, electrical-driven liquid crystal (LC)[43–45] is of tremendous promise to integrate with meta-device and practically exhibit tunable functionality due to its stability, easy-accessibility, and fast modulation rate.

J. Tang, S. Wan, Y. Shi, C. Wan, Z. Wang, Z. Y. Li
Electronic Information School
Wuhan University
Wuhan 430072, China
E-mail: zhongyangli@whu.edu.cn
Z. Y. Li
Wuhan Institute of Quantum Technology
Wuhan 430206, China
Z. Y. Li
School of Microelectronics
Wuhan University
Wuhan 430072, China
The ORCID identification number(s) for the author(s) of this article can be found under https://doi.org/10.1002/adom.202200418.

DOI: 10.1002/adom.202200418

Here, we originally propose and realize a dynamic meta-system for AR holographic display functionality based on layer-folded metasurface integrated with the electrical-driven LC platform. By ingeniously folding the vertical optical path with TIR to incorporate multilayered metasurfaces in parallel onto the same silica substrate surface, we avoid any vertical multi-patterning alignment and successfully cascade a beam-steering metasurface with another two holographic metasurfaces on the same chip surface. Such a layer-folded scheme enjoys single-time lithography processing for multi-patterning with nanoscale alignment accuracy and avoids any vertical alignment issue. More intriguingly, through combining with electrical-driven LC tuning scheme, the design meta-system could actively tune the exhibited far-field holographs as AR dynamic displays in real-time for human eyes. Overall, we believe that the proposed compact layer-folded meta-system with active tuning potential can easily find practical applications for next-generation wearable AR devices, dynamic meta-optics displays, and many others.

2. Results and Discussion

The architectural schematic of the multilayer-folded dynamic meta-system with LC platform integration is shown in **Figure 1**. Based on the layer-folded structural scheme, our design is comprised of a polarization-dependent beam-steering metasurface (in the middle) coupling in parallel with the other two hologram metasurfaces (on each side). When the illumination beam is incident normally onto the middle beam-steering metasurface, it serves to deflect different linear-polarized light to the respective directional side. Through making the beam outgoing angle exceed the critical angle of TIR at the glass/air interface, the whole directional light is refracted and confined within the glass substrate to illuminate onto the side metasurface pattern. Hence, this way effectively cascades the two parallel-placed metasurfaces by such folding vertical optical path scheme. Different holographic display images can be independently encoded into the respective metasurface on each side and projected into human eyes (left and right eye) for dynamic AR display when integrating with the electrical-driven LC platform. Note that the layer-folded metasurface here is indeed separate from the LC cell, where an air gap actually exists between the LC device and the layer-folded metasurface sample.

The unit cell of layer-folded metasurface pattern consists of amorphous silicon (α-Si) rectangular nanoblocks (H = 380 nm, $P_x = P_y$ = 200 nm) on the glass substrate (thickness = 500 µm) with a refractive index of n_1 = 1.45, as shown in **Figure 2**a. By elaborately screening the pattern geometry, we engineer the beam-steering metasurface with optimal conversion efficiency. For normal incidence with linear polarization, we have calculated and screened the transmitted light phase shift and transmittance as a function of length L and width W varying from 60 to 160 nm, as shown in Figure 2b,c. See more details on polarization-dependent beam-steering metasurface in Figure S1 (Supporting Information). The ray-tracing for optical path folding performance is conducted by finite-difference time-domain (FDTD) simulations to verify the precise optical coupling between multi-patterning, as shown in Figure 2d,e. More details on numerical simulation can be found in the Experimental Section. To showcase the essential performance of optical path folding in numerical calculation, the silica substrate thickness here is reduced to 10 µm for the purpose of simplifying the meta-device. To determine the corresponding setting parameters for a supercell containing three nanoblocks, it requires to satisfy $3P_x n_1 \sin\theta_d = m\lambda$ according to the periodic diffraction equation. Hence, for P_x = 200 nm and the incident light wavelength λ = 633 nm in the air, the beam-steering angle θ_d is determined to be ≈46.7° at the diffraction order m of ±1, which noticeably exceeds the critical angle θ_c of 43.6°. Note that the selection of quite small periodicity (P_x = 200 nm) is for the purpose of satisfying the TIR condition. Specifically, for the x-polarized light normal incidence case, the beam is guided along the right-hand

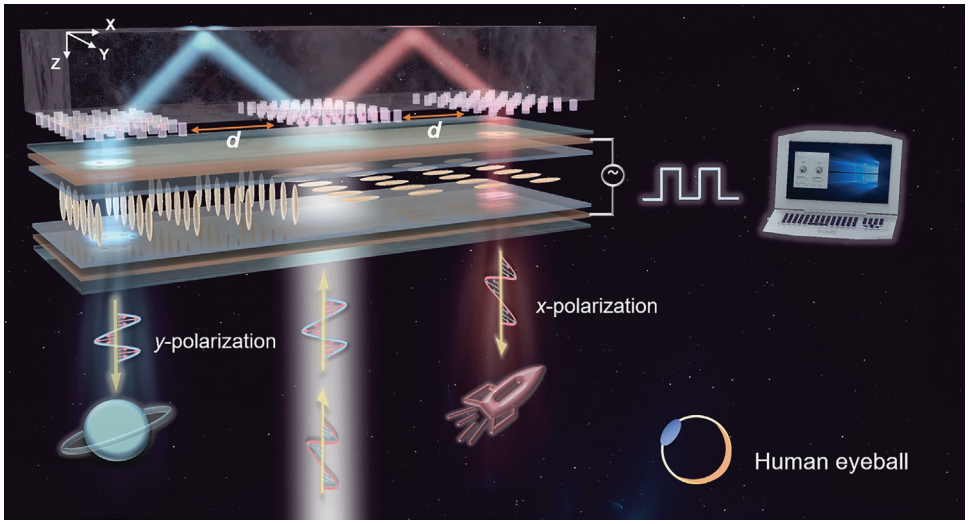

Figure 1. AR meta-system schematics based on the layer-folded metasurface implemented with electrical-driven LC platform. By ingeniously folding the vertical optical path to enable multi-metasurface layers cooperation and coupling, the proposed compact meta-system can dynamically tune AR displays/holographic images to human eyes by electrical-driven LC devices. The gap spacing between the middle beam-steering metasurface and the left/right-side hologram metasurface is d = 710 µm.

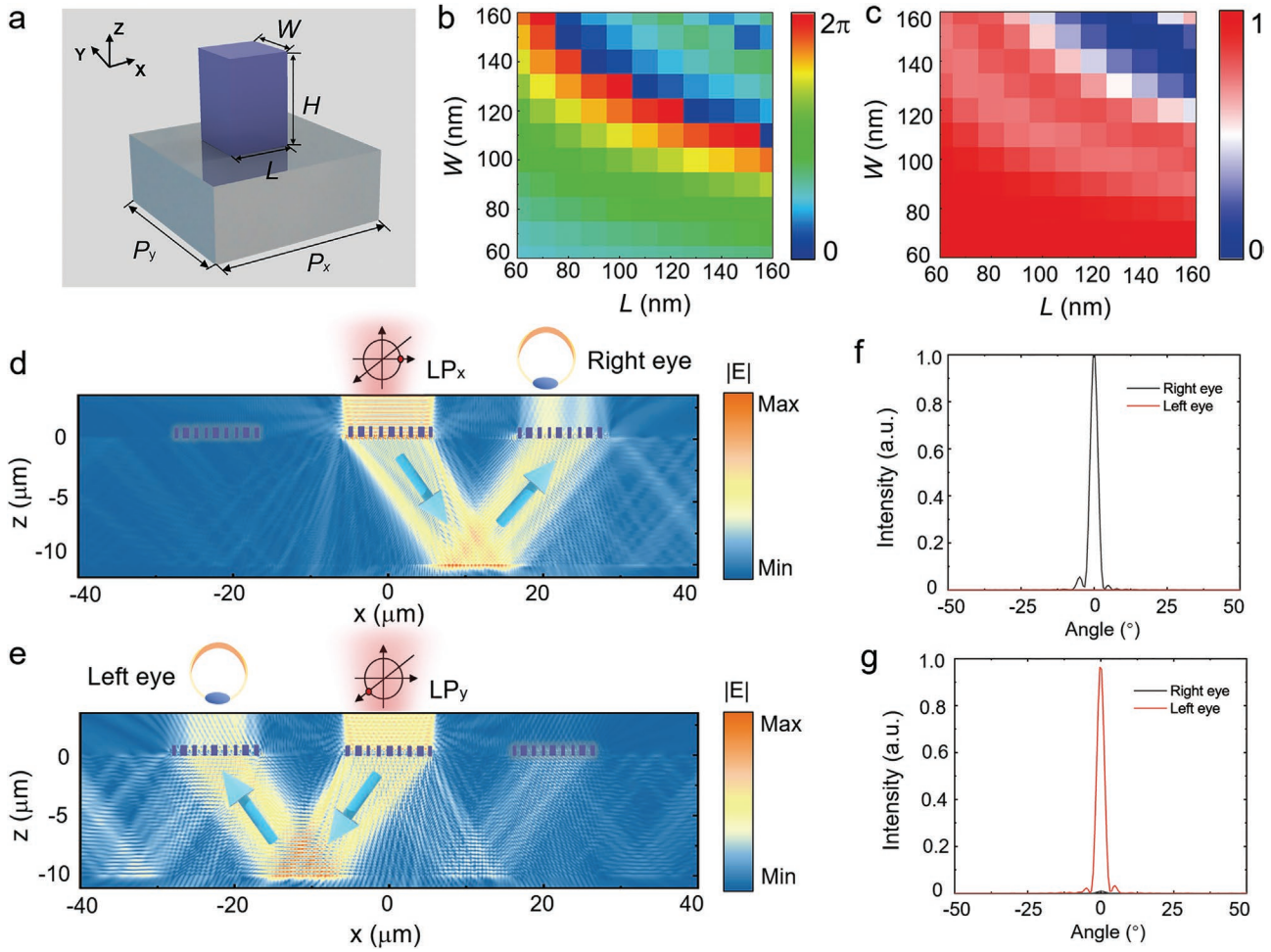

Figure 2. a) Schematics for the unit cell of the nanoblock with height $H = 380$ nm and period $P_x = P_y = 200$ nm. b,c) Simulated 2D map for the phase shift and transmittance for linear polarization as a function of length L and width W at the operation wavelength of 633 nm. d,e) Simulated electric-field amplitude |E| distributions to exhibit the ray-tracing in the layer-folded meta-device for x-/y-polarization at the wavelength of 633 nm, respectively. The x-/y-polarization beam is guided to reflect and propagate to the right-/left-side direction, thus overlapping and coupling with the side metasurface. The blue arrows denote the beam propagation path. f,g) Far-field reflection distribution as a function of the reflected angles for the right-/left-side hologram metasurface, respectively.

side direction (Figure 2d); Likewise, for the y-polarization case, the outgoing direction is switched to the opposite (left-hand side) (Figure 2e). Furthermore, by horizontally cascading with the other two hologram metasurfaces in parallel, it generates a layer-folded meta-system to enable the light field manipulation individually. As shown in Figure 2f,g, the other hologram metasurface on each side is respectively designed to couple with the middle one, exhibiting beam-bending performance to normal direction as a proof-of-concept showcase. The right/left eye (power monitor) shows the high contrast of optical intensity for the normal outgoing direction, thus indicating the independent tuning to exhibit polarization-dependent switching characteristics. As observed that the beam propagation path overlaps with each metasurface pattern, it conquers the long lasting challenge of the vertical alignment requirement and multi-patterns can be fabricated via a single-time lithography process with the spacing accuracy of nanoscale.

To verify the polarization-multiplexing functionality based on the layer-folding meta-device, we have experimentally demonstrated a dual-channel holographic imaging display, as shown in **Figure 3**. By integrating the LC platform into the meta-system, we successfully realized a dynamic tunable holographic display. Figure 3a shows the built-up optical characterization setup to capture the voltage-responsive meta-optics dynamics at the operation wavelength of 633 nm. The fabricated layer-folded metasurface is composed of a middle beam-steering metasurface and two hologram metasurfaces, with a total size of 2420 × 400 μm^2. The middle beam-steering metasurface was fabricated with a sample area of 400 × 400 μm^2, and the left/right-side hologram metasurface is of 300 × 300 μm^2 (1000 × 1000 pixels), with the in-between spacing is 710 μm according to TIR calculation. The corresponding scanning electron microscope (SEM) image of the pattern is shown in Figure 3b. More details on fabrication processing can be found in the Experimental Section. It should be noted that the LC cell device used in our setup was commercially provided by ARCoptix. More detailed parameters of the LC device can be found in the Supporting Information. As we emphasized, the

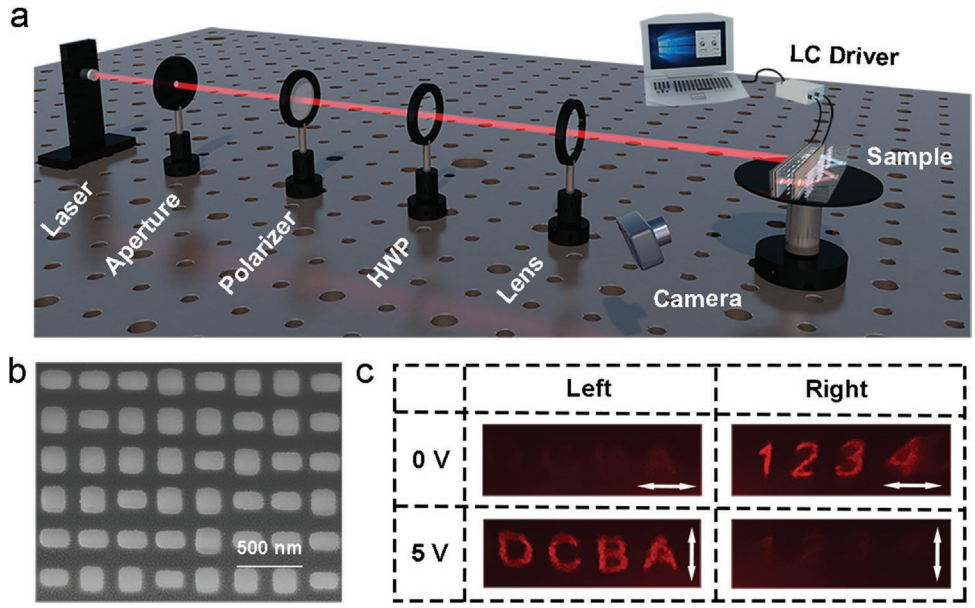

Figure 3. a) Schematic illustration of the optical measurement setup to capture a dual-channel voltage-responsive holographic display. b) A representative SEM image of the holographic metasurfaces. c) Measured dual-channel electrical-tuning meta-holograms projection on the optical opaque screen. The Arabic numbers "1 2 3 4" and English letters "A B C D" can be switchably tuned by applying the external voltage alteration between 0 and 5 V. The inset arrows represent the corresponding *x*-/*y*-polarization beam, respectively.

layer-folded metasurfaces enjoy single-time lithography processing without demanding any precise vertical alignment at the nanoscale. Figure 3c shows the active tuning display of projected dual-channel meta-holography in real-time at different electric-voltage states. Specifically, the holographic image of Arabic numbers "1 2 3 4" is projected onto the far-field optical screen when applying the external voltage of ≈0 V. When the electric voltage is applied to ≈5 V to the LC driver, the original Arabic numbers would disappear, and the projected image is dynamically switched to the English letters "A B C D." Notably, the LC platform is placed between the layer-folded metasurface and the optical screen when the hologram is projected on the far-field optical screen. For dynamic adjusting the LC driver between 0 and 5 V, the corresponding movie for the repeated tuning in real-time can be found in Movie S1 (Supporting Information).

Moreover, the layer-folded metasurface implemented with the LC platform is also successfully demonstrated to enable a dynamic AR display meta-system for human eyes, as shown in **Figure 4**a. Here, the mixture of floating virtual images and real-world scenes can be simultaneously captured with the switchable ability for the individual human eye. To verify such AR performance, we utilized a mobile phone camera to record, as shown in Figure 4b,c. When applying the external electrical state at 0 V, the floating Arabic numbers of "7 8" are exhibited and immersed in the real-world background. On the contrast of 5 V input, the floating images are switched to the exhibiting

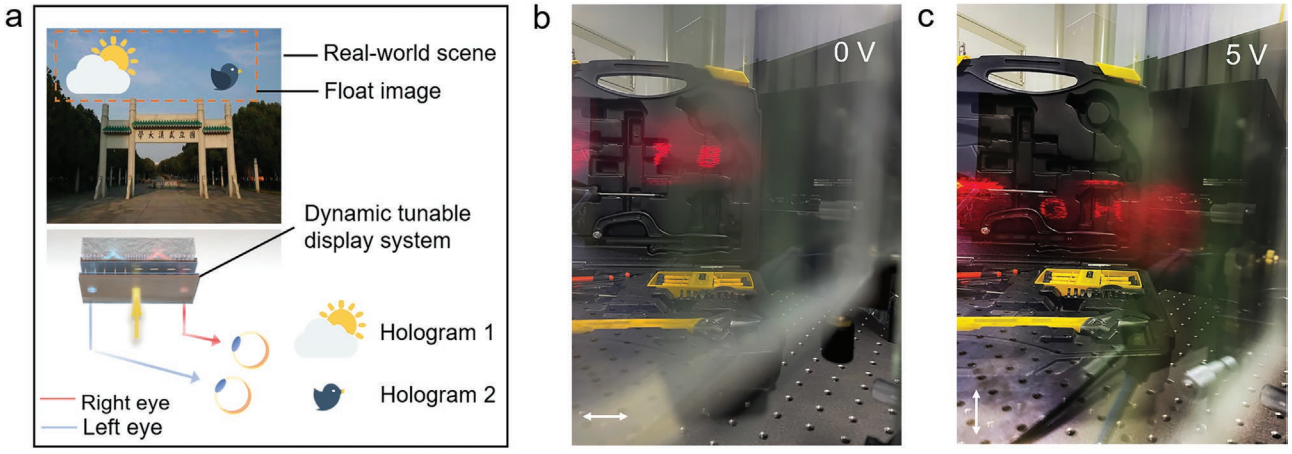

Figure 4. a) Conceptual illustration for the dynamic AR meta-system based on a layer-folded metasurface scheme integrated with the tunable LC platform. b,c) Switchable AR exhibitions of Arabic number "7 8" or English letters "G H" are dynamically switchable, immersing in the real-world scene by applying a tunable voltage of 0 or 5 V. The inset arrows represent the corresponding *x*-/*y*-polarization beam.

letters of "G H". See Movie S2 (Supporting Information) for the dynamic process in real-time.

3. Conclusion

In summary, we have proposed and demonstrated a dynamic tunable AR display meta-system based on layer-folded metasurfaces integrated with the LC platform. By cascading a beam-steering metasurface in parallel with another two hologram metasurfaces on the same surface, the vertical optical space can be ingeniously folded in order to effectively avoid the accurate vertical alignment demand between multi-patterning, thus promisingly paving a new way to create more complicated meta-systems. Furthermore, by integrating with the LC platform and leveraging its real-time tunable characteristics for polarized light, we have achieved the holographic AR dynamic display in the real-world scene. Future work can be extended to realize the dynamic 3D vision by encoding two stereoscopic images into the projected holographs. Overall, such proposed meta-system based on layer-folding scheme with LC platform integration suggest various promising applications in the next-wearable AR display system, multi-functional optical devices, and photonic integrated circuits.

4. Experimental Section

Sample Fabrication: A 380 nm thick of α-Si was deposited onto the 500 µm thick fused silica substrate via plasma-enhanced chemical vapor deposition (PECVD). The PMMA resist was spin-coated and baked at 150 °C for 3 min, then a conductive polymer was also spin-coated and baked at 90 °C for 3 min to prevent charge accumulation. The pattern of α-Si nanoantenna designs was exposed by utilizing EBL (Raith eLINE Plus, 20 kV). Then the PMMA resist at 20 °C for 80 s was developed to ensure the highest resolution patterns. A 20 nm thick chromium (Cr) as a dry-etch mask was deposited by thermal evaporation. After the lift-off process in acetone removed the PMMA resists, the patterns of Cr hard mask were transferred to α-Si by using reactive ion etching (RIE) and then removed by Cr etchant.

Numerical Simulation: The FDTD method to perform numerical simulation was utilized. A unit cell composed of α-Si nanoblock on the top of a glass substrate (n_1 = 1.45) was simulated using periodic boundary conditions along the *x*-/*y*-axis and perfect match layers along the *z*-direction to obtain the phase shift. For ray-tracing simulation, Gaussian beam was only incident on the middle metasurface, and the electrical distribution was collected with a 2D power monitor at *x*-*z* plane. Two power monitors were placed above the left-/right-side hologram metasurface to collect the far-field. Periodic boundary conditions were applied along the *y*-axis and perfect match layers conditions for the *x*-/*z*-direction.

Supporting Information

Supporting Information is available from the Wiley Online Library or from the author.

Acknowledgements

J.T. and S.W. contributed equally to this work. The authors gratefully acknowledge Hubei Province Funds for Distinguished Young Scientists (2021CFA043), Wuhan Science and Technology Bureau (2020010601012196), Recruitment Program of Global Experts (501100010871), Start-up Program of Wuhan University (501100007046). This work was supported by the Center for Nanoscience and Nanotechnology at Wuhan University and Hubei Luojia Laboratory.

Conflict of Interest

The authors declare no conflict of interest.

Data Availability Statement

The data that support the findings of this study are available from the corresponding author upon reasonable request.

Keywords

layer-folded metasurface, liquid crystals, meta-holography, multi-patterning alignment, switchable AR display, total internal reflection

Received: February 22, 2022
Revised: March 24, 2022
Published online: May 11, 2022

[1] Y. Liang, H. Lin, K. Koshelev, F. Zhang, Y. Yang, J. Wu, Y. Kivshar, B. Jia, *Nano Lett.* **2021**, *21*, 1090.
[2] J. Tian, Q. Li, P. A. Belov, R. K. Sinha, W. Qian, M. Qiu, *ACS Photonics* **2020**, *7*, 1436.
[3] M. Liu, W. Zhu, P. Huo, L. Feng, M. Song, C. Zhang, L. Chen, H. J. Lezec, Y. Lu, A. Agrawal, T. Xu, *Light: Sci. Appl.* **2021**, *10*, 107.
[4] J. Jang, T. Badloe, Y. Yang, T. Lee, J. Mun, J. Rho, *ACS Nano* **2020**, *14*, 15317.
[5] J. Tang, Z. Li, S. Wan, Z. Wang, C. Wan, C. Dai, Z. Li, *ACS Appl. Mater. Interfaces* **2021**, *13*, 38623.
[6] J. Tao, Q. You, Z. Li, M. Luo, Z. Liu, Y. Qiu, Y. Yang, Y. Zeng, Z. He, X. Xiao, G. Zheng, S. Yu, *Adv. Mater.* **2021**, *34*, 2106080.
[7] Z. Li, C. Wan, C. Dai, J. Zhang, G. Zheng, Z. Li, *Adv. Opt. Mater.* **2021**, *9*, 2100297.
[8] F. Zhao, R. Lu, X. Chen, C. Jin, S. Chen, Z. Shen, C. Zhang, Y. Yang, *Laser Photonics Rev.* **2021**, *15*, 2100097.
[9] M. Y. Shalaginov, S. An, Y. Zhang, F. Yang, P. Su, V. Liberman, J. B. Chou, C. M. Roberts, M. Kang, C. Rios, Q. Du, C. Fowler, A. Agarwal, K. A. Richardson, C. Rivero-Baleine, H. Zhang, J. Hu, T. Gu, *Nat. Commun.* **2021**, *12*, 1225.
[10] C. Wan, Z. Li, S. Wan, C. Dai, J. Tang, Y. Shi, Z. Li, *Adv. Funct. Mater.* **2021**, *32*, 2110592.
[11] R. Kaissner, J. Li, W. Lu, X. Li, F. Neubrech, J. Wang, N. Liu, *Sci. Adv.* **2021**, *7*, 9450.
[12] T. Wu, X. Zhang, Q. Xu, E. Plum, K. Chen, Y. Xu, Y. Lu, H. Zhang, Z. Zhang, X. Chen, G. Ren, L. Niu, Z. Tian, J. Han, W. Zhang, *Adv. Opt. Mater.* **2022**, *10*, 2101223.
[13] Y. Eliezer, G. Qu, W. Yang, Y. Wang, H. Yilmaz, S. Xiao, Q. Song, H. Cao, *Light: Sci. Appl.* **2021**, *10*, 104.
[14] C. Dai, C. Wan, Z. Li, Z. Wang, R. Yang, G. Zheng, Z. Li, *Adv. Opt. Mater.* **2021**, *9*, 2100950.
[15] S. Wan, C. Wan, C. Dai, Z. Li, J. Tang, G. Zheng, Z. Li, *Adv. Opt. Mater.* **2021**, *9*, 2101547.
[16] Z. Wang, C. Dai, J. Zhang, D. Wang, Y. Shi, X. Wang, G. Zheng, X. Zhang, Z. Li, *Adv. Funct. Mater.* **2021**, *32*, 2110022.

[17] I. Kim, H. Jeong, J. Kim, Y. Yang, D. Lee, T. Badloe, G. Kim, J. Rho, *Adv. Opt. Mater.* **2021**, *9*, 2100609.
[18] I. Kim, K. Kim, M. A. Ansari, M. Q. Mehmood, T. Badloe, Y. Kim, J. Gwak, H. Lee, Y. Kim, J. Rho, *Sci. Adv.* **2021**, *7*, 9943.
[19] J. Song, S. Huang, Y. Ma, Q. Cheng, R. Hu, X. Luo, *Opt. Express* **2020**, *28*, 875.
[20] W. Xi, Y. Liu, J. Song, R. Hu, X. Luo, *Opt. Lett.* **2021**, *46*, 888.
[21] M. Mansouree, H. Kwon, E. Arbabi, A. McClung, A. Faraon, A. Arbabi, *Optica* **2020**, *7*, 77.
[22] D. Frese, Q. Wei, Y. Wang, L. Huang, T. Zentgraf, *Nano Lett.* **2019**, *19*, 3976.
[23] H. Kwon, E. Arbabi, S. M. Kamali, M. Faraji-Dana, A. Faraon, *Nat. Photonics* **2019**, *14*, 109.
[24] S. Tan, F. Yang, V. Boominathan, A. Veeraraghavan, G. V. Naik, *ACS Photonics* **2021**, *8*, 1421.
[25] S. Divitt, W. Zhu, C. Zhang, J. Lezec Henri, A. Agrawal, *Science* **2019**, *364*, 890.
[26] A. Arbabi, E. Arbabi, Y. Horie, S. M. Kamali, A. Faraon, *Nat. Photonics* **2017**, *11*, 415.
[27] J. Kim, D. Jeon, J. Seong, T. Badloe, N. Jeon, G. Kim, J. Kim, S. Baek, J. L. Lee, J. Rho, *ACS Nano* **2022**, *16*, 3546.
[28] Y. Hu, X. Luo, Y. Chen, Q. Liu, X. Li, Y. Wang, N. Liu, H. Duan, *Light: Sci. Appl.* **2019**, *8*, 86.
[29] P. Georgi, Q. Wei, B. Sain, C. Schlickriede, Y. Wang, L. Huang, T. Zentgraf, *Sci. Adv.* **2021**, *7*, 9718.
[30] Y. Chen, Z. Shu, S. Zhang, P. Zeng, H. Liang, M. Zheng, H. Duan, *Int. J. Extreme Manuf.* **2021**, *3*, 032002.
[31] M. Faraji-Dana, E. Arbabi, H. Kwon, S. M. Kamali, A. Arbabi, J. G. Bartholomew, A. Faraon, *ACS Photonics* **2019**, *6*, 2161.
[32] M. Faraji-Dana, E. Arbabi, A. Arbabi, S. M. Kamali, H. Kwon, A. Faraon, *Nat. Commun.* **2018**, *9*, 4196.
[33] I. Kim, M. A. Ansari, M. Q. Mehmood, W. S. Kim, J. Jang, M. Zubair, Y. K. Kim, J. Rho, *Adv. Mater.* **2020**, *32*, 2004664.
[34] C. Zou, A. Komar, S. Fasold, J. Bohn, A. A. Muravsky, A. A. Murauski, T. Pertsch, D. N. Neshev, I. Staude, *ACS Photonics* **2019**, *6*, 1533.
[35] J. Wang, K. Li, H. He, W. Cai, J. Liu, Z. Yin, Q. Mu, V. K. S. Hisao, D. Gérard, D. Luo, G. Li, Y. J. Liu, *Laser Photonics Rev.* **2021**, *16*, 2100396.
[36] Y. Hu, X. Ou, T. Zeng, J. Lai, J. Zhang, X. Li, X. Luo, L. Li, F. Fan, H. Duan, *Nano Lett.* **2021**, *21*, 4554.
[37] Y. Liu, J. Song, W. Zhao, X. Ren, Q. Cheng, X. Luo, N. X. Fang, R. Hu, *Nanophotonics* **2020**, *9*, 855.
[38] Y. Ma, D. Sikdar, A. Fedosyuk, L. Velleman, M. Zhao, L. Tang, A. A. Kornyshev, J. B. Edel, *ACS Appl. Mater. Interfaces* **2019**, *11*, 22754.
[39] Z. Wang, L. Jiang, X. Li, B. Li, S. Zhou, Z. Xu, L. Huang, *ACS Appl. Mater. Interfaces* **2021**, *13*, 51736.
[40] R. Hu, W. Xi, Y. Liu, K. Tang, J. Song, X. Luo, J. Wu, C.-W. Qiu, *Mater. Today* **2021**, *45*, 120.
[41] S. C. Malek, H. S. Ee, R. Agarwal, *Nano Lett.* **2017**, *17*, 3641.
[42] Y. Gao, C. Huang, C. Hao, S. Sun, L. Zhang, C. Zhang, Z. Duan, K. Wang, Z. Jin, N. Zhang, A. V. Kildishev, C. W. Qiu, Q. Song, S. Xiao, *ACS Nano* **2018**, *12*, 8847.
[43] M. Sharma, T. Ellenbogen, *Laser Photonics Rev.* **2020**, *14*, 2000253.
[44] M. Sharma, N. Hendler, T. Ellenbogen, *Adv. Opt. Mater.* **2020**, *8*, 1901182.
[45] S. Q. Li, X. Xu, R. Maruthiyodan Veetil, V. Valuckas, R. Paniagua-Domínguez, A. I. Kuznetsov, *Science* **2019**, *364*, 1087.